frontiers | Frontiers in Earth Science

ORIGINAL RESEARCH
published: 13 April 2022
doi: 10.3389/feart.2022.859471

Historic Earthquakes for the Xianshuihe Fault Derived From Lake Mugeco in the Southeastern Margin of the Tibetan Plateau During the Past 300 Years

Liyuan Liu[1], *Jingxuan Yang*[1], *Xingqi Liu*[1]*, *Xin Mao*[2] *and Rong Qin*[1]

[1]College of Resource Environment and Tourism, Capital Normal University, Beijing, China, [2]Institute of Hydrogeology and Environmental Geology, Chinese Academy of Geological Sciences, Shijiazhuang, China

The lacustrine deposition with continuity and chronological reliability is one of the important archives to establish paleo-seismic sequences. In this study, sediment short cores were obtained from Lake Mugeco, located in the Selaha section of the Xianshuihe fault zone on the southeastern margin of the Tibetan Plateau. The chronology is established using $^{210}Pb/^{137}Cs$ and AMS^{14}C dating results. Seismic events are identified based on sedimentary characteristics (color, density, and grain size), organic matter content, and high-resolution XRF element scanning data for the past 300 years. There are four whitish turbidites in the sediments of Lake Mugeco, which are characterized by a high content of clay fraction and detrital elements (K, Rb, Ca, Sr, Ti, and Si) and low organic matter content. These four turbidites were dated in 1944–1956 C.E., 1919–1932 C.E., 1673–1837 C.E., and 1507–1739 C.E., with dating errors, possibly corresponding to large historical earthquakes of 1955 (M_S 7.5), 1932 (M_S 6), 1786 (M_S 7 ¾), and 1725 (M_S 7) recorded in the Selaha section of the Xianshuihe fault zone. This study provides scientific evidence for further reconstructing longer-temporal seismic events in the Xianshuihe fault zone inferred from sediments of Lake Mugeco.

Keywords: lacustrine sediment, seismic event, Xianshuihe fault, Lake Mugeco, turbidite

OPEN ACCESS

Edited by:
Shiyong Yu,
Jiangsu Normal University, China

Reviewed by:
Gueorgui Ratzov,
Université Côte d'Azur, France
Pierre Sabatier,
University of Savoie-Mont Blanc, France
Fuyuan An,
Qinghai Normal University, China

***Correspondence:**
Xingqi Liu
xqliu@cnu.edu.cn

Specialty section:
This article was submitted to Quaternary Science, Geomorphology and Paleoenvironment, a section of the journal Frontiers in Earth Science

Received: *21 January 2022*
Accepted: *07 March 2022*
Published: *13 April 2022*

Citation:
Liu L, Yang J, Liu X, Mao X and Qin R (2022) Historic Earthquakes for the Xianshuihe Fault Derived From Lake Mugeco in the Southeastern Margin of the Tibetan Plateau During the Past 300 Years. Front. Earth Sci. 10:859471. doi: 10.3389/feart.2022.859471

INTRODUCTION

The Xianshuihe fault zone is regarded as one of the most tectonically active regions with high seismicity in China (Wen et al., 2008; Bai et al., 2018). Historical earthquake data and instrumental monitoring have recorded more than 20 earthquake events with a magnitude of $M_s \geq 6.5$ since 1700 C.E., over ten of which have a magnitude of above M_s 7.0 (Writing Group of Compilation of Sichuan Earthquake Data, 1980a; Writing Group of Compilation of Sichuan Earthquake Data, 1980b; Wen et al., 1989). Previous studies have discerned the paleoseismic events and inferred their recurrence periodicity and interval of strong earthquakes through techniques of trenching and dating in the Xianshuihe fault zone for the past 20,000 years (Sun et al., 2007; Liang, 2019).

Continuous lacustrine sediments can provide supplementary information to whole earthquake records in an active fault zone (Ghazoui et al., 2019; Vandekerkhove et al., 2019; Fan et al., 2020; Hubert-Ferrari et al., 2020; Gastineau et al., 2021; Wils et al., 2021). Seismic shaking can induce subaqueous slope failure and remobilization of surficial, previously deposited sediments to be

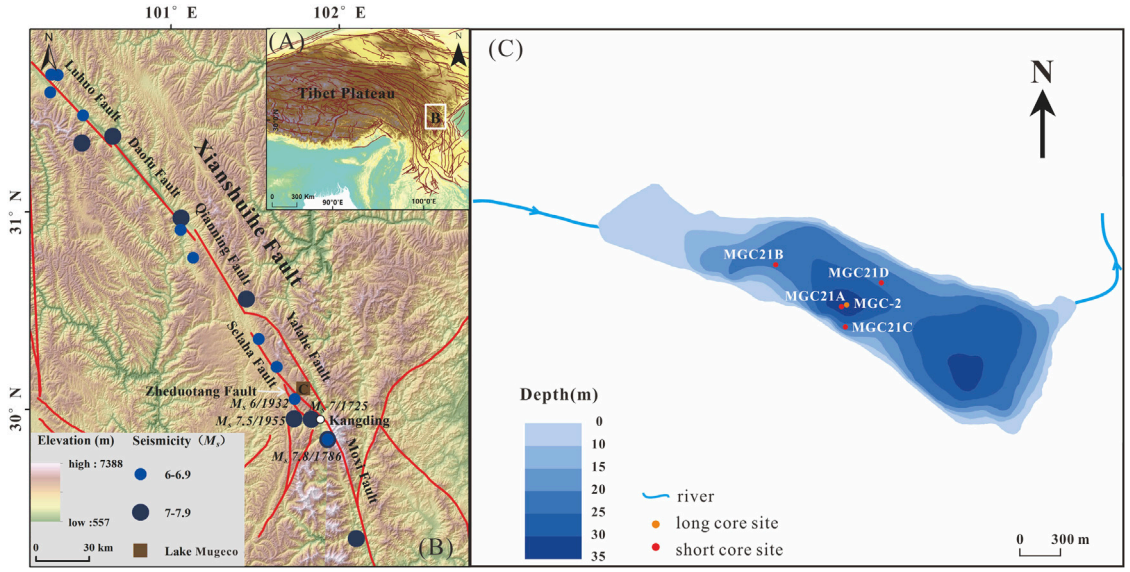

FIGURE 1 | Location of the study area. Location of the Xianshuihe fault in TP **(A)**. Seven fault segments and historical earthquakes along the fault **(B)**. Bathymetric map of Lake Mugeco and the location of sediment cores **(C)**.

transformed into the subaqueous turbidity currents and debris or mudflows flowing into the lakebed (Bryn et al., 2005; Moernaut et al., 2017; Praet et al., 2017). It may also trigger sedimentary instabilities such as onshore landslides and deltaic slope failures, resulting in mobilized masses and turbidity currents (Howarth et al., 2014; Van Daele et al., 2015). Sediment formed by these earthquake-induced turbidity currents is called seismoturbidite or homogenite (Sturm et al., 1995; Chapron et al., 1999; Shiki et al., 2000; Beck, 2009; Howarth et al., 2014; Van Daele et al., 2015; Moernaut et al., 2018; Lu et al., 2021; Polonia et al., 2021). Moreover, an earthquake can induce deformation, such as microfaults (Topal and Ozkul, 2014; Avşar et al., 2015; Jiang et al., 2016), microfolds (Monecke et al., 2004), liquefaction, and flowage (Beck, 2009; Topal and Ozkul, 2014). In addition, earthquake-induced water oscillation (i.e., seiche) can erode shallow material or resuspend sediments from the steepening parts of the lake basin and form oscillating bottom currents, influencing *in situ* soft sediment deformation and mass-transport deposits (Alsop and Marco, 2012; Lu et al., 2020). However, the aforementioned characteristics of sedimentation are not generated only by seismic events, as rainstorms and windstorms caused by climate change and spontaneous landslides due to overloading of subaqueous slopes can also result in sedimentary disturbances (Chassiot et al., 2016a; Kinder, et al., 2019; Rapuc et al., 2020; Sabatier et al., 2017; Wilhelm et al., 2012; Wilhelm et al., 2022; Wils et al., 2021). Therefore, it is crucial to correctly distinguish seismic events from other events preserved in lake sediments. Here, we first establish the chronology based on ^{210}Pb/^{137}Cs and accelerator mass spectrometry (AMS) ^{14}C dating of a short core from Lake Mugeco. Then, the sedimentary characteristics (including sediment color, density, and grain size), organic matter, and element content are employed to identify event layers preserved in several short cores from Lake Mugeco. Finally, four earthquake events different from one flood event are identified on short lake sediment cores that span a period with known historical earthquake and flood events.

STUDY AREA

The Xianshuihe fault is a giant left-lateral strike-slip fault on the southeastern margin of the Tibetan Plateau (TP) (**Figures 1A,B**). At Huiyuan Monastery, the fault is halved into NW and SE sections based on their respective structural styles (Qian et al., 1988; Wen et al., 1989). The former, with a simple geologic structure, includes the Luhuo segment, the Daofu segment, and the Qianning segment, while the latter, with complicated construction, consists of the Yalahe segment, Selaha segment, Zheduotang segment, and Moxi segment to the south of Kangding city (**Figure 1B**). It is considered that the Xianshuihe fault was formed 2–13 Ma ago and the cumulative length of slip reaches ~60 km (Roger et al., 1995; Wang et al., 1998; Wang et al., 2012; Yan and Lin, 2015). The long-term horizontal slip rate of 10–20 mm/yr estimated by different scholars is explicitly higher than others in southeastern margin of TP (Allen et al., 1991; Qiao et al., 2004; Xiong et al., 2010), so the Xianshuihe fault is regarded as a high-velocity strike-slip fault.

Lake Mugeco (30°08′N, 101°50′E) is located in Yala Town of North Kangding city, Sichuan Province, near the Selaha segment of the mid-Xianshuihe fault (**Figure 1B**). Formed by regional taphrogeny and dispersion, the lake is the largest fault lake on the Xianshuihe fault. There is a steep slope bounding the southeastern side of the basin that Lake Mugeco fills, and relatively flat terrain in the northwest. The NW-SE major

direction of the lake basin is consistent with the extensions of the Xianshuihe fault (**Figure 1C**). The batholith is dominated by medium-coarse-grained granite in the catchment. Controlled by the fault of the Selaha segment, intensive shattering spreads out and extensive fractures develop on the southwest bank of the basin (Zhou et al., 2001). Lake Mugeco lies in the transitional zone between the East Asian Summer Monsoon and the Indian Summer Monsoon region. Meteorological data from Kangding station (30°1′48″ N, 101°34′48″) show that mean annual temperature is 7.2°C and mean annual precipitation is 830 mm with most of the annual precipitation falling from May to September. Lake Mugeco and its catchment cover an area of 1.8 and 75 km^2, respectively, (Hu et al., 2015; Sun et al., 2015; 2016). The lake is at an elevation of 3780 m. The maximum water depth we measured in 2020 was 34.4 m. It is a hydrologically open lake, mainly fed by a river from the northwest. There is one outlet flowing into the Yala River on the northeast side of the lake (**Figure 1C**) (Sun et al., 2016; Ni et al., 2019).

MATERIALS AND METHODS

Sediment Coring

In July 2019, a 3.9-m-long sediment core (MGC-2) from the centre of Lake Mugeco was recovered by an Uwitec drilling platform at a depth of 30.5 m (**Figure 1C**). Then, in May 2021, four short sediment cores were obtained using a piston gravity corer at different depths varying from 23 to 30.5 m. These short cores were respectively named of MGC21A (31 cm-long), MGC21B (27 cm-long), MGC21C (25 cm-long), and MGC21D (32 cm-long) (**Figure 1C**).

Laboratory Analysis

All short sediment cores were split along the central axis with a core-cutting machine in our laboratory. Halved cores were photographed, and the lithology was described. This study focuses mainly on short-core MGC21A for dating, XRF core scanning, and analyses of grain size, total organic carbon (TOC), and total nitrogen (TN). For MGC21B, MGC21C, and MGC21D, XRF core scanning was used to get X-radiographic images and element variations.

$^{210}Pb/^{137}Cs$ and ^{14}C Dating

The subsamples of core MGC21, sampled at intervals of 0.5 cm, were vacuum freeze dried for 48 h, then ground to powder as fine as ca 150 μm with a mortar and pestle. The activities of ^{137}Cs, ^{226}Ra, and ^{210}Pb of the samples at different depth were measured by Ortec high purity germanium gamma spectrometer. Herein the excess ^{210}Pb activity ($^{210}Pb_{ex}$) was computed by subtracting the ^{226}Ra activity from the total activity of ^{210}Pb, as ^{226}Ra was assumed to be in equilibrium with supported ^{210}Pb ($^{210}Pb_{sup}$). The constant flux constant sedimentation rate (CFCS) model method is given to estimate sediment age within ca 150 years (Appleby and Oldfield, 1978; Robbins, 1978; Bruel and Sabatier, 2020). Plant remains were selected at a depth of 50 cm from the long core MGC-2 for AMS^{14}C dating at Beta Analytic Testing Laboratory, United States.

XRF Core Scanning

The surfaces of halved cores were smoothed to give a flat surface and covered with a thin Ultralene film to prevent desiccation during core scanning. The cores were scanned by the Itrax Core Scanner (Cox Analytical Instruments) equipped with an Rh X-ray tube to get optical images, X-radiographic images, and element variations. A voltage of 60 kV, a current of 35 mA, a step size of 20 μm and an exposure time of 200 ms were set to get X-radiographic images. A voltage of 30 kV, a current of 55 mA, a step size of 200 μm and an exposure time of 5 s were set to get element variations expressed as counts per second (CPS). Elements with low raw counts are excluded, as they are close to the detection limits of ITRAX and may be even measurement noise. In order to avoid the matric effect, a centered log-ratio (CLR) transformation was applied to calibrate the elements (Weltje et al., 2015). Principal component analysis (PCA) is a statistical approach that can transform a large number of variables (concentration of elements) into fewer independent variables (Sabatier et al., 2010). PCA is performed by SPSS software.

Measurement of Grain Size

Samples of core MGC21A were sliced at 0.5 cm intervals, and ~0.5 g wet samples were used for the measurement of grain size. For the removal of organic matter and carbonates, samples were pretreated with 10% H_2O_2 and with 10% HCl, and then dispersed in an ultrasonic vibrator for 15–20 min with 10% $(NaPO_3)_6$. Last, the grain-size distributions of the MGC21A core were measured using a Malvern Mastersizer 3,000 laser grain-size analyzer.

Measurement of TOC and TN

About 1 g of samples were first treated with 10% HCl to remove carbonates, rinsed with deionized water, and dried in the drying oven prior to analysis. The dried samples were ground into 100-μm-fine powder. Finally, ~3–5-mg samples were analyzed by the EURO EA 3,000 elemental analyzer to determine TOC and TN content.

RESULT

Sedimentary Characteristics

The deposits of the MGC21A core mainly consist of greyish-brown and light greyish-black clayey silt. Percentages of silt and clay range from 75.15 to 85.13% and 13.37–23.15%, with an average of 82.34 and 16.09%, respectively (**Figure 2**). The proportion of sand is less than 2.96% on average. It is found that the variation of clay is the opposite to that of silt. Also, the median diameter ranges from 9.33–11.40 μm with an average of 10.37 μm, in accordance with the variation of silt. Besides, Rad values are associated with grain size variations, which means that overall low Rad values respond to high content of clay fraction, and vice versa (**Figure 2**). There are three whitish layers presented as dark bands in the X-radiographic image at the depths of 6.5, 17, and 22 cm in the MGC21A core (shown as E1, E3, and E4 in **Figure 2**). They are also characterized by relatively high clay content and low silt content, and the median diameter and Rad values decrease correspondingly as well. At a depth of 9.5 to

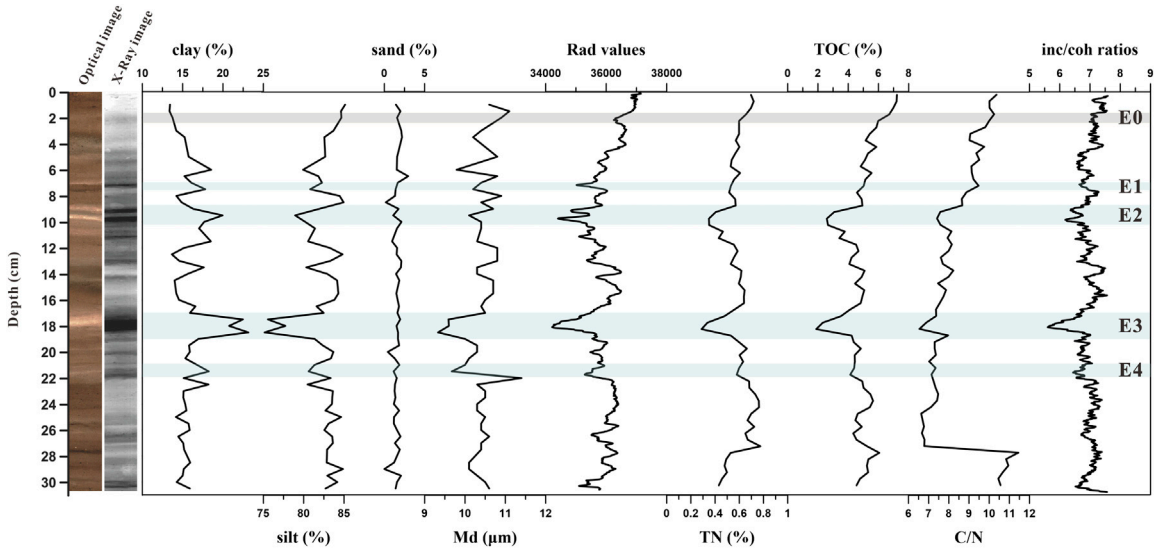

FIGURE 2 | Optical and X-radiographic images, and different proxy variations with depth in the core MGC21A. E0- flood event labeled as a light grey bar; E1, E2, E3, and E4- earthquake events labeled as light blue bars.

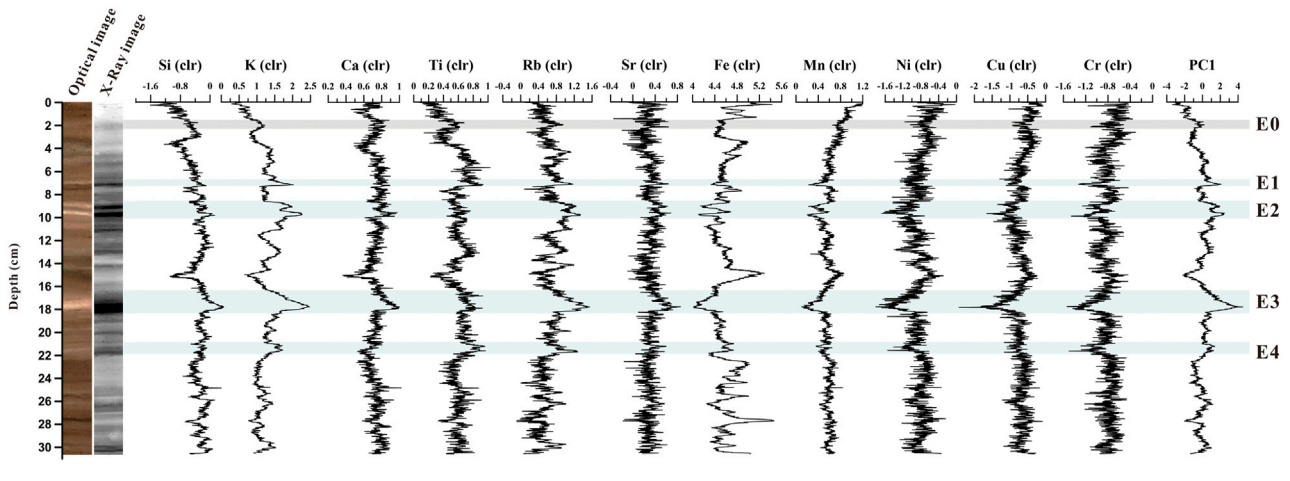

FIGURE 3 | Variations of element contents and PC1 values in the core MGC21A. E0- flood event; E1, E2, E3, and E4- earthquake events.

8.5 cm, there are two whitish layers characterized by dark bands in the X-radiographic image and low Rad values. Due to the closeness of these two layers, we named them E2 (**Figure 2**). Given that the resolution of grainsize is low, clay and silt content do not have variations, but X-radiographic images present dark and Rad values decrease in the E0 layer.

TOC, TN, C/N Ratio, and Inc/coh

In the core MGC21A, the contents of TOC and TN vary from 1.88 to 7.22% and from 0.29 to 0.78%, respectively, and their variations are consistent with each other. Carbon/nitrogen atomic (C/N) ratios are generally less than 10 (**Figure 2**). The incoherent/coherent scattering intensity ratios (inc/coh ratios) display a similar trend with TOC and TN as well (**Figure 2**). Contents of TOC, TN, and inc/coh ratios rapidly decrease in E2–E4 layers while they do not show obvious decreasing trend in E0 and E1 due to their thin layer or low resolution of TOC and TN (**Figure 2**). E2 also shows a double wiggle on variations of inc/coh ratios.

Element Variations

Variations of elements transformed by CLR in the core MGC21A are shown in **Figure 3**. PCA results show that the first two principal components together capture 65.29% of the variance (PC 1: 55.64%, PC 2: 9.65%) (**Figure 4A**). PCA 1 has positive loadings for elements of K, Rb, Ca, Sr, Ti, and Si, most of which

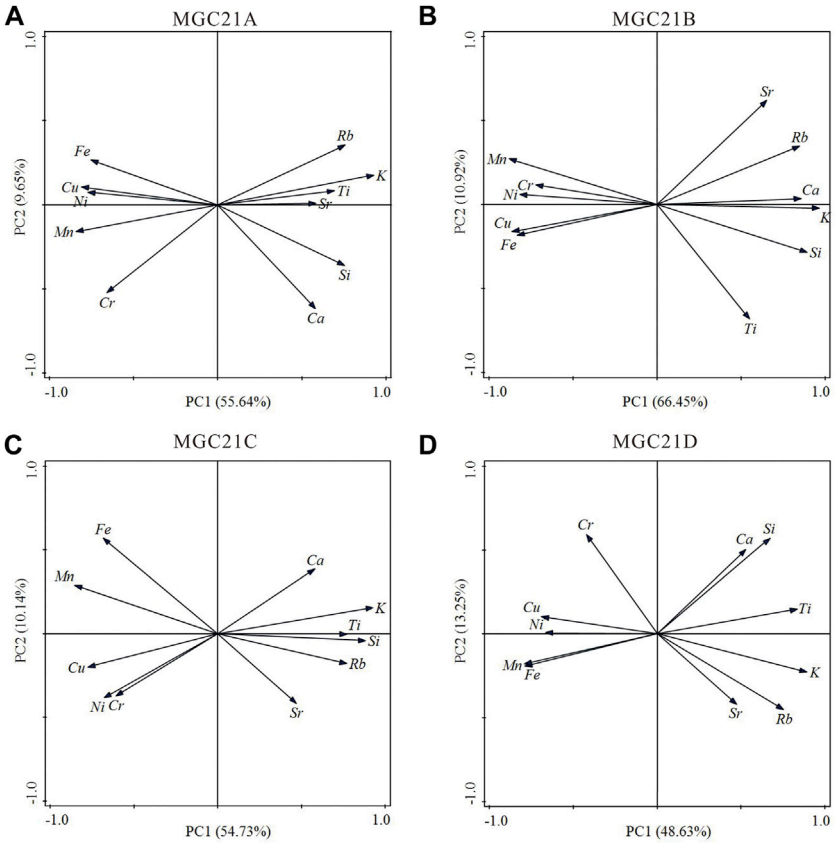

FIGURE 4 | PCA results in the cores MGC21A **(A)**, MGC21B **(B)**, MGC21C **(C)**, and MGC21D **(D)**.

belong to detrital elements. PCA 2 has positive loadings for Fe and negative loadings for Mn (**Figure 4A**), possibly reflecting the redox status of Mugeco Lake. It is discovered that the contents of K, Rb, Ca, Sr, Ti, Si, and PCA 1 values increase sharply in the base of four whitish layers and decrease upward, labeled as E0, E1, E3, and E4, especially in the E1, E3, and E4 layers (**Figure 3**). E2 also shows a double wiggle on the content of detrital elements and PC 1 values (**Figure 3**).

Generally, there are the same sedimentary characteristics in the E1, E2, E3, and E4 layers. The sediment colors in these layers turn white, and their dark X-radiographic images suggest increasing clay content (Croudace et al., 2006), decreasing median diameter, a higher density, and lower Rad values than other parts (**Figure 2**). As the sediment accumulation rate of the core is very low (0.91 mm/yr) and the highest resolution we can achieve for grainsize analysis is at a 0.5 cm interval, which spans ca. 6 years, it is impossible for grainsize data to show the graded bed with coarser sediment at the base finning upward in E0–E4 layers. However, the coarse sediment fractions are often rich in detrital elements (K, Rb, Ca, Sr, Ti, and Si), which can reflect the mm-scale changes in grain size (Avşar et al., 2014; Gastineau et al., 2021; Wilhelm et al., 2022). Sharp increasing of these detrital elements and PCA 1 values in the base of E1–E4 layers and decreasing upward well indicate coarser sediment at the base finning upward, which suggests that E1–E4 layers are characterized by turbidites. In order to avoid the one-core occasionality and to validate the universality of E0–E4 layers, three short cores (i.e., MGC21B, MGC21C, and MGC21D) in different parts of Lake Mugeco were analyzed and compared with the core MGC21A (**Figure 2**). It is found that all short cores contain five layers characterized by darker X-radiographic images, decreased Rad values, and PC 1 representing detrital element content (**Figures 4B–D**), and decreased inc/coh ratios, which can represent organic matter content (**Figure 5**).

Sediment Chronology

A logarithmic plot of $^{210}Pb_{ex}$ activity shows a general linear trend with depth (**Figure 6A**). The exponential decay pattern of $^{210}Pb_{ex}$ activity along the depth is employed to develop a chronology by applying the CFCS model (Bruel and Sabatier, 2020), indicating a low sediment accumulation rate (SAR) of 0.91 mm/yr (**Figure 6A**). The artificial isotope ^{137}Cs has been mainly released from atomic bomb tests, nuclear industrial emissions, or accidents (Foucher et al., 2021). After release, it can enter the atmosphere, and then be precipitated and preserved on land or water. The ^{137}Cs activity increases upward from the depth of 7 cm in the core of MGC21A and reaches its highest values (~160 Bq/kg) at 5 cm (**Figure 6A**), which could be related to the most intense period of nuclear

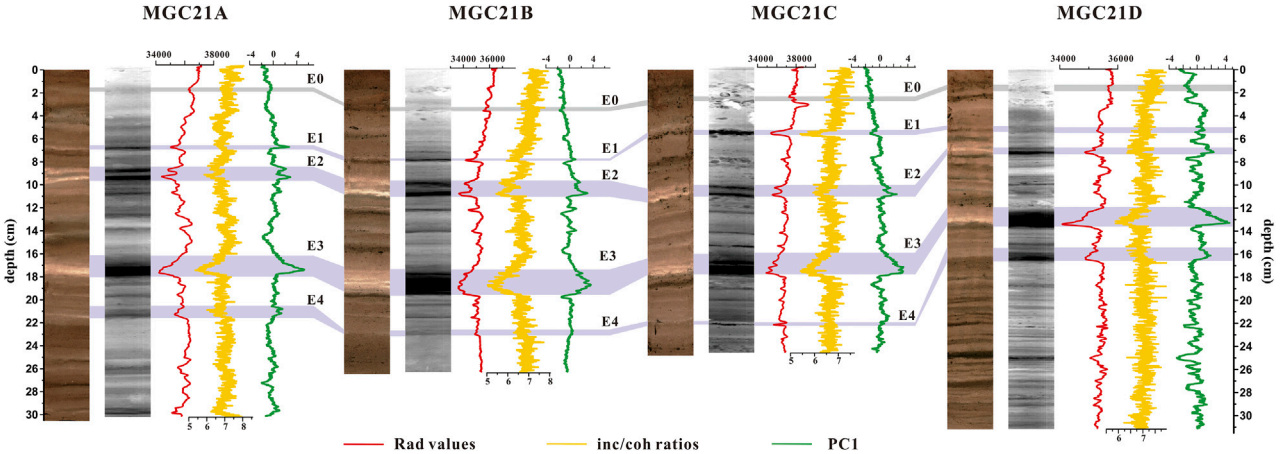

FIGURE 5 | Comparison of E0-E4 event layers characterized by Rad values, inc/coh ratios, and PC1 among the different cores in Lake Mugeco.

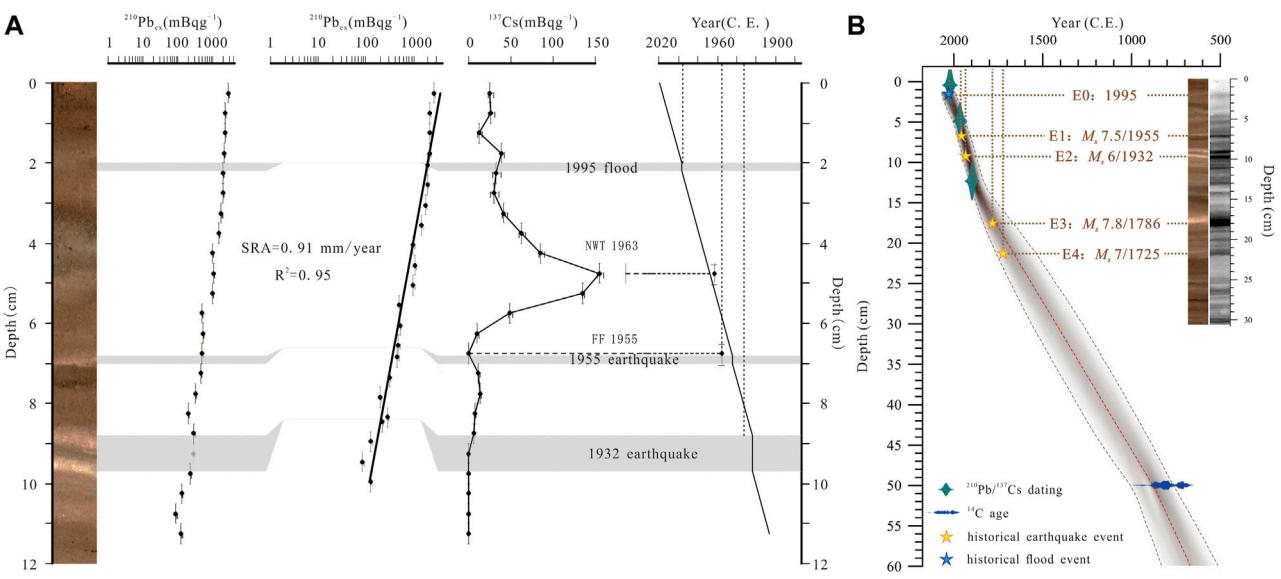

FIGURE 6 | Chronology model for cores MGC21A and MGC-2. $^{210}Pb/^{137}Cs$ dating results of the core MGC21A **(A)**. Age-depth model derived from $^{210}Pb/^{137}Cs$ dating of the core MGC21A and AMS^{14}C dating of the core MGC-2 **(B)**. E0- flood event; E1, E2, E3, and E4- earthquake events.

testfallout. And the values gradually decrease upward from a depth of 5 cm. Nuclear tests started in 1955 C.E. and reached their climax around 1963 C.E. (Foucher et al., 2021), thus the peak at 5 cm-depth is fixed at 1963 C.E. (**Figure 6A**) (Norris et al., 1994). The ^{137}Cs age of 1963 C.E. at 5 cm is consistent with the CFCS model result (**Figure 6A**). The ^{14}C age dated on the plant remains at 50 cm in the long core MGC-2 parallel to the short core MGC21A, which is 1230 ± 30 BP. Combined with the age model derived from $^{210}Pb/^{137}Cs$ and AMS^{14}C dating, the chronology is established by the Bacon 2.5.7 procedure in R software using the Bayesian method (Blaauw and Christen, 2011; Reimer et al., 2020) for the upper 50 cm sediment of Lake Mugeco (**Figure 6B**).

DISCUSSION

Seismic Events Recorded in Lake Mugeco

Previous studies indicate that turbidites can be produced by flood, landslide, deltaic collapse, or earthquake (Brocard et al., 2014; Ghazoui et al., 2019; Vandekerkhove et al., 2019; Wils et al., 2021). Flood-induced turbidities usually contain multitudes of allochthonous detrital materials and present a fining-upward unit and a better sorting in grain-size (Vandekerkhove et al., 2019; Zhang et al., 2015). Furthermore, floods and landslides have a short recurrence interval (Archer et al., 2019). It was documented that lasting heavy precipitation in June and July 1995 caused rising water levels in the Yala River and Zheduo River, which

originates from Lake Mugeco and Gongga Mountain, respectively. This heavy precipitation induced a flood occurring in 1995 in Kangding city that has encountered the most serious flood since 1776 (Xie et al., 1997). E0 at a depth of ~2.0 cm in the core of MGC21A is characterized by a dark X-radiographic image, a slight decrease in Rad and inc/coh ratios, and an increase in PC1 and elements of K, Rb, Ca, Sr, Ti, and Si. The E0 layer in other short cores also has the same characteristics. The $^{137}Cs/^{210}Pb$ dating suggests that the E0 layer is dated to 1995–1998 C.E. and was presumably triggered by the flood in 1995 (**Figure 6A**). The proxies in the E0 layer are similar to those in the E1–E4 layers (**Figure 5**), but have much little variations, which indicate that the E1–E4 layers are impossible to trigger by a flood event. Landslide-induced subaqueous deposits are generally rich in terrestrial organic matter (Avşar et al., 2014; Bussmann and Anselmetti, 2010), but with low C/N ratios in E1–E4 layers, that organic matter is endogenous (**Figure 3**). So, the E1–E4 layers are not landslide-induced deposits in Lake Mugeco. Turbidites induced by slope failure are either similar to or coarser than the background sediment as they originate in the slope areas (Moernaut et al., 2014; Van Daele et al., 2015; Wilhelm et al., 2016). E1–E4 layers with higher clay content indicate that they are unlikely to be induced by slope failure (**Figure 2**).

At the bottom of turbidite layers, there is a sharp increase in detrital element content at the base and fine-grained matter in these layers (**Figures 2**, **3**, **5**). In terms of these observations, we suggest that E1–E4 turbidite layers in Lake Mugeco are considered the result of earthquake-induced seiches (Chapron et al., 1999; Rapuc et al., 2018; Schwab et al., 2009). Beck (2009) and Aurelia et al. (2013) attributed fine-grained whitish muddy turbidites to earthquake-induced subaqueous deposits (Aurelia et al., 2013; Beck, 2009). Due to the small and narrow surface of Lake Mugeco, the seiches are prone to being triggered when an earthquake takes place (Avşar et al., 2014; Barberopoulou, 2006). Seiche waves erode surface materials from the lakeshore, and coarse grains are moved and then deposited in shoal water while separated and suspended fine grains are transported to the central lake. Meanwhile, the surficial soft sediments on the lakebed are remobilised and resuspended. Under the effect of gravity separation, fine grains are precipitated more slowly than coarse ones, and transformed into a whitish silt homogenites layer that is rich in detrital elements. From XRF core scanning, inc/coh ratios usually increase in agreement with concentrated organic matter (Woodward and Gadd, 2019), and thus Woodward et al. (2018) used inc/coh ratio as a proxy index of organic matter to reveal seismic events recorded in Lake Chappa'ai in the Southern Alps, New Zealand (Woodward et al., 2018). However, the MGC21A core shows a decrease in the inc/coh ratios, TOC and TN contents in E1–E4 layers, which means that during the formation of homogenites, suspending organic matter is oxidised and decomposed in the water column before precipitation (Schwestermann et al., 2020). Moreover, the lower C/N ratio in E1–E4 layers could indicate a lacustrine origin through mass reworked deposits related to earthquake-trigged seiches rather than a terrestrial origin characterized by higher C/N attributed to floods (**Figure 2**) (Howarth et al., 2012).

Chronology of Seismic Activities Matched With Historic Records

To further validate that the deposits in the E1, E2, E3, and E4 event layers of MGC21A were generated by earthquakes, their ages based on our chronology model were compared with the records of past earthquakes occurring in the study area. Four turbidite layers (E1-E3) are dated to 1944–1956 C.E., 1919–1932 C.E., 1673–1837C.E., and 1507–1739 C.E. respectively (**Figure 6A**). On April 14th, 1955,a M_s 7.5 earthquake happened in the Zheduotang segment (101.8°E, 30°N) to the 17 km southeast of Lake Mugeco (**Figure 1B**), its shaking intensity was measured as X at the epicentre and VII in the study area referring to the Chinese Seismic Intensity Scale (1980) (Wang et al., 1996; Yan et al., 2019). This earthquake produced a 43-km-long surface rupture to the east of the epicentre, spreading from Kangding to Wasigou, where the seismic intensity was also measured as VII. Such natural hazards as collapse, landslides, and rockfall were also triggered at Nanmenguan and Angzhou, in Luding County to the southeast (Wang et al., 1996). Based on the ^{137}Cs and ^{210}Pb chronology, the E1 layer may coincide with the M_s 7.5 earthquake in 1955 (**Figure 6A**). According to data from the National Earthquake Data Center, there was another M_s 6.0 earthquake in southwest Ganzi County, Sichuan Province (101.8°E, 30.1°N) on 3rd May, 1932. The epicentre was only about 7 km from Lake Mugeco, and the earthquake intensity exceeds VII. As there were no other earthquakes from 1919 to 1932 C.E., the E2 layer, which consists of two whitish layers, may be an amalgamated turbidite resulting from a synchronous trigger by an earthquake in 1932. There were M_s 7.8 and M_s 7.0 earthquakes with the earthquake intensity of IX at the epicentre in Dajianlu (nowadays known as Kangding) on 1st June 1786, and on 1st August, 1725, respectively (Writing Group of "Compilation of Sichuan Earthquake Data", 1980) (**Figure 1B**). Based on the chronology model (**Figure 6B**), the E3 and E4 layers are possibly related to the M_s 7.8 and M_s 7.0 earthquakes in 1786 and 1725, respectively. Generally, within dating errors, E1–E4 layers coincide with the M_s 7.5 earthquake in 1955, the M_s 6.0 earthquake of 1932, the M_s 7.8 earthquake in 1786, and the M_s 7.0 earthquake in 1725, respectively (**Figure 6**).

The sensitivity of the lacustrine sediment to seismic activity depends on the magnitude of the earthquake and the distance between the position of the lake and the epicentre. Chassiot et al. (2016b) found that maar Lake Pavin was imprinted by earthquakes with a seismic intensity of Vwithin a 15-km radius. Ghazoui et al. (2019) discovered that a minimum M_s 5.6 earthquake within a 15-km radius or more than a M_s 6.5 earthquake within an 80-km radius could be recorded by the sediment of Lake Rara (Ghazoui et al., 2019). It was shown that earthquake-triggered water oscillation (seiche) occurs when the earthquake magnitude exceeds 7.0 (Alsop & Marco, 2012; Avşar et al., 2014). Although there are lots of earthquakes with different magnitudes around Lake Mugeco, only four earthquakes of M_s 6.0–7.5 within a 40-km radius have been well-preserved in the sediment of Lake Mugeco, and the earthquake

intensity has been greater than VII in Lake Mugeco during the last 300 years. It is clear that Lake Mugeco can only record strong earthquakes with a short epicentre distance.

CONCLUSION

Lacustrine deposits are mainly composed of greyish–brown and light greyish–black silt in Lake Mugeco over the past 300 years. There are four obvious turbidite layers characterized by highly-dense whitish silt, low content of organic matter, high content of clay fraction, and detrital elements (K, Rb, Ca, Sr, Ti, and Si). The formation of these four turbidite layers is related to seiche-triggered erosion of the lakeshore and sedimentation after subaqueous surficial sediment remobilization and resuspension. Chronological results reveal that the ages of the turbidite layers are compatible with four seismic events along the Selaha segment of the Xianshuihe fault zone, i.e., M_s 7.5 earthquake in 1955, M_s 6.0 earthquake in 1932, M_s 7.8 earthquake in 1786, and M_s 7.0 earthquake in 1725. Although historical records show that there are frequent earthquakes over M_s 6.0 along the Xianshuihe fault, only earthquakes with seismic intensities from VII to VIII within a 40-km radius can be recorded by lacustrine sediments in Lake Mugeco. Our study can provide scientific evidence for a long-term paleoseismic reconstruction along the Xianshuihe fault based on lacustrine sediments of Lake Mugeco.

DATA AVAILABILITY STATEMENT

The raw data supporting the conclusions of this article will be made available by the authors without undue reservation.

AUTHOR CONTRIBUTIONS

LL and XL designed this study; RQ and XM analyzed the data; LL and JY wrote the manuscript; and LL, XL, and XM polished the paper. All authors approved the final version of the manuscript.

FUNDING

This work was financially supported by a corporative project of the National Natural Science Foundation of China (NSFC) and the German Research Foundation (DFG) (Grant No. 41861134030).

REFERENCES

Allen, C. R., Zhuoli, L., Hong, Q., Xueze, W., Huawei, Z., and Weishi, H. (1991). Field Study of a Highly Active Fault Zone: The Xianshuihe Fault of Southwestern China. *Geol. Soc. Amer. Bull.* 103 (9), 1178–1199. doi:10.1130/0016-7606(1991)103<1178:fsoaha>2.3.co;2

Alsop, G. I., and Marco, S. (2012). Tsunami and Seiche-Triggered Deformation within Offshore Sediments. *Sediment. Geology.* 261-262, 90–107. doi:10.1016/j.sedgeo.2012.03.013

Appleby, P. G., and Oldfield, F. (1978). The Calculation of lead-210 Dates Assuming a Constant Rate of Supply of Unsupported 210Pb to the Sediment. *Catena* 5 (1), 1–8. doi:10.1016/S0341-8162(78)80002-2

Archer, C., Noble, P., Rosen, M. R., Sagnotti, L., Florindo, F., Mensing, S., et al. (2019). Lakes as Paleoseismic Records in a Seismically-Active, Low-Relief Area (Rieti Basin, Central Italy). *Quat. Sci. Rev.* 211, 186–207. doi:10.1016/j.quascirev.2019.03.004

Aurelia, H.-F., Ulas, A., Meriam El, O., Gilles, L., Philippe, M., and Nathalie, F. (2013). Paleoseismic Record Obtained by Coring a Sag-Pond along the North Anatolian Fault (Turkey). *Ann. Geophys.* 55 (5), 929–953. doi:10.4401/ag-5460

Avşar, U., Hubert-Ferrari, A., De Batist, M., Lepoint, G., Schmidt, S., and Fagel, N. (2014). Seismically-triggered Organic-Rich Layers in Recent Sediments from Göllüköy Lake (North Anatolian Fault, Turkey). *Quat. Sci. Rev.* 103, 67–80. doi:10.1016/j.quascirev.2014.08.020

Avşar, U., Hubert-Ferrari, A., De Batist, M., Schmidt, S., and Fagel, N. (2015). Sedimentary Records of Past Earthquakes in Boraboy Lake during the Last Ca 600 Years (North Anatolian Fault, Turkey). *Palaeogeogr. Palaeoclimatol. Palaeoecol.* 433, 1–9. doi:10.1016/j.palaeo.2015.04.031

Bai, M., Chevalier, M.-L., Pan, J., Replumaz, A., Leloup, P. H., Métois, M., et al. (2018). Southeastward Increase of the Late Quaternary Slip-Rate of the Xianshuihe Fault, Eastern Tibet. Geodynamic and Seismic Hazard Implications. *Earth Planet. Sci. Lett.* 485, 19–31. doi:10.1016/j.epsl.2017.12.045

Barberopoulou, A. (2006). Long-Period Effects of the Denali Earthquake on Water Bodies in the Puget Lowland: Observations and Modeling. *Bull. Seismological Soc. America* 96 (2), 519–535. doi:10.1785/0120050090

Beck, C. (2009). "Late Quaternary Lacustrine Paleo-Seismic Archives in north-western Alps: Examples of Earthquake-Origin Assessment of Sedimentary Disturbances". *Earth-Science Rev.* 96 (4), 327–344. doi:10.1016/j.earscirev.2009.07.005

Blaauw, M., and Christen, J. A. (2011). Flexible Paleoclimate Age-Depth Models Using an Autoregressive Gamma Process. *Bayesian Anal.* 6 (3), 457–474. doi:10.1214/ba/1339616472

Brocard, G., Adatte, T., Magand, O., Pfeifer, H.-R., Bettini, A., Arnaud, F., et al. (2014). The Recording of Floods and Earthquakes in Lake Chichój, Guatemala during the Twentieth century. *J. Paleolimnol.* 52 (3), 155–169. doi:10.1007/s10933-014-9784-4

Bruel, R., and Sabatier, P. (2020). Serac: an R Package for ShortlivEd RAdionuclide Chronology of Recent Sediment Cores. *J. Environ. Radioactivity* 225, 106449. doi:10.1016/j.jenvrad.2020.106449

Bryn, P., Berg, K., Forsberg, C. F., Solheim, A., and Kvalstad, T. J. (2005). Explaining the Storegga Slide. *Mar. Pet. Geol.* 22 (1-2), 11–19. doi:10.1016/b978-0-08-044694-3.50005-6

Bussmann, F., and Anselmetti, F. S. (2010). Rossberg Landslide History and Flood Chronology as Recorded in Lake Lauerz Sediments (Central Switzerland). *Swiss J. Geosci.* 103 (1), 43–59. doi:10.1007/s00015-010-0001-9

Chapron, E., Beck, C., Pourchet, M., and Deconinck, J.-F. (1999). 1822 Earthquake-Triggered Homogenite in Lake Le Bourget (NW Alps). *Terra Nova* 11 (2-3), 86–92. doi:10.1046/j.1365-3121.1999.00230.x

Chassiot, L., Chapron, E., Di Giovanni, C., Albéric, P., Lajeunesse, P., Lehours, A.-C., et al. (2016a). Extreme Events in the Sedimentary Record of Maar Lake Pavin: Implications for Natural Hazards Assessment in the French Massif Central. *Quat. Sci. Rev.* 141, 9–25. doi:10.1016/j.quascirev.2016.03.020

Chassiot, L., Chapron, E., Di Giovanni, C., Lajeunesse, P., Tachikawa, K., Garcia, M., et al. (2016b). Historical Seismicity of the Mont Dore Volcanic Province (Auvergne, France) Unraveled by a Regional Lacustrine Investigation: New Insights about Lake Sensitivity to Earthquakes. *Sediment. Geology.* 339, 134–150. doi:10.1016/j.sedgeo.2016.04.007

Croudace, I. W., Rindby, A., and Rothwell, R. G. (2006). ITRAX: Description and Evaluation of a New Multi-Function X-Ray Core Scanner. *Geol. Soc. Lond. Spec. Publications* 267 (1), 51–63. doi:10.1144/GSL.SP.2006.267.01.04

Fan, J., Jiang, H., Shi, W., Guo, Q., Zhang, S., Wei, X., et al. (2020). A 450-year Lacustrine Record of Recurrent Seismic Activities Around the Fuyun Fault,

Altay Mountains, Northwest China. *Quat. Int.* 558, 75–88. doi:10.1016/j.quaint.2020.08.051

Foucher, A., Chaboche, P.-A., Sabatier, P., and Evrard, O. (2021). A Worldwide Meta-Analysis (1977-2020) of Sediment Core Dating Using Fallout Radionuclides Including ^{137}Cs and $^{210}Pb_{xs}$. *Earth Syst. Sci. Data* 13, 4951–4966. doi:10.5194/essd-13-4951-2021

Gao, S., Chen, L., Liang, M., Wang, D., Li, Y., Han, M., et al. (2021). Rupture Characteristics and Seismic Recurrence Behaviors of Xianshuihe Fault Revealed by Xinyulin Trenches, South of Kangding. *Adv. Eng. Sci.* 53, 53–61. doi:10.15961/j.jsuese.202100031

Gastineau, R., Sigoyer, J., Sabatier, P., Fabbri, S. C., Anselmetti, F. S., Develle, A. L., et al. (2021). Active Subaquatic Fault Segments in Lake Iznik along the Middle Strand of the North Anatolian Fault, NW Turkey. *Tectonics* 40 (1), e2020TC00640. doi:10.1029/2020tc006404

Ghazoui, Z., Bertrand, S., Vanneste, K., Yokoyama, Y., Nomade, J., Gajurel, A. P., et al. (2019). Potentially Large Post-1505 AD Earthquakes in Western Nepal Revealed by a Lake Sediment Record. *Nat. Commun.* 10 (1), 2258. doi:10.1038/s41467-019-10093-4

Howarth, J. D., Fitzsimons, S. J., Norris, R. J., and Jacobsen, G. E. (2012). Lake Sediments Record Cycles of Sediment Flux Driven by Large Earthquakes on the Alpine Fault, New Zealand. *Geology* 40 (12), 1091–1094. doi:10.1130/g33486.1

Howarth, J. D., Fitzsimons, S. J., Norris, R. J., and Jacobsen, G. E. (2014). Lake Sediments Record High Intensity Shaking that Provides Insight into the Location and Rupture Length of Large Earthquakes on the Alpine Fault, New Zealand. *Earth Planet. Sci. Lett.* 403, 340–351. doi:10.1016/j.epsl.2014.07.008

Hu, Z., Anderson, N. J., Yang, X., Zhang, E., Wang, R., and Jones, R. T. (2015). Climate and Tectonic Effects on Holocene Development of an Alpine Lake (Muge Co, SE Margin of Tibet). *The Holocene* 26 (5), 801–813. doi:10.1177/0959683615618263

Hubert-Ferrari, A., Lamair, L., Hage, S., Schmidt, S., Çağatay, M. N., and Avşar, U. (2020). A 3800 Yr Paleoseismic Record (Lake Hazar Sediments, Eastern Turkey): Implications for the East Anatolian Fault Seismic Cycle. *Earth Planet. Sci. Lett.* 538, 116152. doi:10.1016/j.epsl.2020.116152

Jiang, H., Zhong, N., Li, Y., Xu, H., Yang, H., and Peng, X. (2016). Soft Sediment Deformation Structures in the Lixian Lacustrine Sediments, Eastern Tibetan Plateau and Implications for Postglacial Seismic Activity. *Sediment. Geology.* 344, 123–134. doi:10.1016/j.sedgeo.2016.06.011

Kinder, M., Tylmann, W., Rzeszewski, M., and Zolitschka, B. (2019). Varves and Mass-Movement Deposits Record Distinctly Different Sedimentation Dynamics since the Late Glacial (Lake Szurpiły, Northeastern Poland). *Quat. Res.* 93, 299–313. doi:10.1017/qua.2019.61

Liang, M. (2019). *Characteristics of the Late-Quaternary Fault Activity of the Xianshuihe Fault*. PhD Thesis. Beijing: Institute of Geology, China Earthquake Administration. doi:10.27489/d.cnki.gzdds.2019.000019

Lu, Y., Wetzler, N., Waldmann, N., Agnon, A., Biasi, G. P., and Marco, S. (2020). A 220,000-Year-Long Continuous Large Earthquake Record on a Slow-Slipping Plate Boundary. *Sci. Adv.* 6 (48), eaba4170. doi:10.1126/sciadv.aba4170

Lu, Y., Moernaut, J., Bookman, R., Waldmann, N., Wetzler, N., Agnon, A., et al. (2021). A New Approach to Constrain the Seismic Origin for Prehistoric Turbidites as Applied to the Dead Sea Basin. *Geophys. Res. Lett.* 48 (3), e2020GL090947. doi:10.1029/2020gl090947

Monecke, K., Anselmetti, F. S., Becker, A., Sturm, M., and Giardini, D. (2004). The Record of Historic Earthquakes in Lake Sediments of Central Switzerland. *Tectonophysics* 394 (1-2), 21–40. doi:10.1016/j.tecto.2004.07.053

Moernaut, J., Daele, M. V., Heirman, K., Fontijn, K., Strasser, M., Pino, M., et al. (2014). Lacustrine Turbidites as a Tool for Quantitative Earthquake Reconstruction: New Evidence for a Variable Rupture Mode in South central Chile. *J. Geophys. Res. Solid Earth* 119 (3), 1607–1633. doi:10.1002/2013jb010738

Moernaut, J., Van Daele, M., Strasser, M., Clare, M. A., Heirman, K., Viel, M., et al. (2017). Lacustrine Turbidites Produced by Surficial Slope Sediment Remobilization: A Mechanism for Continuous and Sensitive Turbidite Paleoseismic Records. *Mar. Geology.* 384, 159–176. doi:10.1016/j.margeo.2015.10.009

Moernaut, J., Van Daele, M., Fontijn, K., Heirman, K., Kempf, P., Pino, M., et al. (2018). Larger Earthquakes Recur More Periodically: New Insights in the Megathrust Earthquake Cycle from Lacustrine Turbidite Records in South-central Chile. *Earth Planet. Sci. Lett.* 481, 9–19. doi:10.1016/j.epsl.2017.10.016

Ni, Z., Jones, R., Zhang, E., Chang, J., Shulmeister, J., Sun, W., et al. (2019). Contrasting Effects of Winter and Summer Climate on Holocene Montane Vegetation Belts Evolution in Southeastern Qinghai-Tibetan Plateau, China. *Palaeogeogr. Palaeoclimatol. Palaeoecol.* 533, 109232. doi:10.1016/j.palaeo.2019.06.005

Norris, R. S., Burrows, A. S., and Fieldhouse, R. W. (1994). *British, French, and Chinese Nuclear Weapons*. Boulder, Colorado: Westview Press, 333–336.

Polonia, A., Bonetti, C., Bonetti, J., Çağatay, M. N., Gallerani, A., Gasperini, L., et al. (2021). Deciphering Co-seismic Sedimentary Processes in the Mediterranean Sea Using Elemental, Organic Carbon, and Isotopic Data. *Geochem. Geophys. Geosyst.* 22 (7), e2020GC009446. doi:10.1029/2020gc009446

Praet, N., Moernaut, J., Van Daele, M., Boes, E., Haeussler, P. J., Strupler, M., et al. (2017). Paleoseismic Potential of Sublacustrine Landslide Records in a High-Seismicity Setting (South-central Alaska). *Mar. Geology.* 384, 103–119. doi:10.1016/j.margeo.2016.05.004

Qian, H., Allen, C. R., Luo, Z., Wen, X., Zhou, H., and Huang, W. (1988). The Active Characteristics of Xianshuihe Fault in the Holocence. *Earthquake Res. Chin.* 4 (02), 11–20.

Qiao, X., Wang, Q., and Du, R. (2004). Characteristics of Current Crustal Deformation of Active Blocks in the Sichuan-Yunnan Region. *Chin. J. Geophys.* 47 (05), 806–812. doi:10.1002/cjg2.568

Rapuc, W., Sabatier, P., Andrič, M., Crouzet, C., Arnaud, F., Chapron, E., et al. (2018). 6600 Years of Earthquake Record in the Julian Alps (Lake Bohinj, Slovenia). *Sedimentology* 65 (5), 1777–1799. doi:10.1111/sed.12446

Rapuc, W., Jacq, K., Develle, A.-L., Sabatier, P., Fanget, B., Perrette, Y., et al. (2020). XRF and Hyperspectral Analyses as an Automatic Way to Detect Flood Events in Sediment Cores. *Sediment. Geology.* 409, 105776. doi:10.1016/j.sedgeo.2020.105776

Reimer, P. J., Austin, W. E. N., Bard, E., Bayliss, A., Blackwell, P. G., Bronk Ramsey, C., et al. (2020). The IntCal20 Northern Hemisphere Radiocarbon Age Calibration Curve (0-55 Cal kBP). *Radiocarbon* 62 (4), 725–757. doi:10.1017/rdc.2020.41

Robbins, J. A. (1978). "Geochemical and Geophysical Applications of Radioactive lead," in *The Biogeochemistry of Lead in the Environment*. Editor J. O. Nriagu (Amsterdam: Elsevier), 285–393.

Roger, F., Calassou, S., Lancelot, J., Malavieille, J., Mattauer, M., Zhiqin, X., et al. (1995). Miocene Emplacement and Deformation of the Konga Shan Granite (Xianshuihe Fault Zone, West Sichuan, China): Geodynamic Implications. *Earth Planet. Sci. Lett.* 130 (1-4), 201–216. doi:10.1016/0012-821X(94)00252-T

Sabatier, P., Dezileau, L., Briqueu, L., Colin, C., and Siani, G. (2010). Clay Minerals and Geochemistry Record from Northwest Mediterranean Coastal Lagoon Sequence: Implications for Paleostorm Reconstruction. *Sediment. Geology.* 228 (3-4), 205–217. doi:10.1016/j.sedgeo.2010.04.012

Sabatier, P., Wilhelm, B., Ficetola, G. F., Moiroux, F., Poulenard, J., Develle, A.-L., et al. (2017). 6-kyr Record of Flood Frequency and Intensity in the Western Mediterranean Alps - Interplay of Solar and Temperature Forcing. *Quat. Sci. Rev.* 170, 121–135. doi:10.1016/j.quascirev.2017.06.019

Schwab, M. J., Werner, P., Dulski, P., McGee, E., Nowaczyk, N. R., Bertrand, S., et al. (2009). Palaeolimnology of Lake Sapanca and Identification of Historic Earthquake Signals, Northern Anatolian Fault Zone (Turkey). *Quat. Sci. Rev.* 28 (11-12), 991–1005. doi:10.1016/j.quascirev.2009.02.018

Schwestermann, T., Huang, J., Konzett, J., Kioka, A., Wefer, G., Ikehara, K., et al. (2020). Multivariate Statistical and Multiproxy Constraints on Earthquake-Triggered Sediment Remobilization Processes in the Central Japan Trench. *Geochem. Geophys. Geosyst.* 21 (6), e2019GC008861. doi:10.1029/2019GC008861

Shiki, T., Kumon, F., Inouchi, Y., Kontani, Y., Sakamoto, T., Tateishi, M., et al. (2000). Sedimentary Features of the Seismo-Turbidites, Lake Biwa, Japan. *Sediment. Geol.* 135 (1-4), 37–50. doi:10.1016/S0037-0738(00)00061-0

Sturm, M., Siegenthaler, C., and Pickrill, R. A. (1995). "Turbidites and 'homogenites,". *A Conceptual Model of Flood and Slide Deposits* (Paris: Publication IAS-16th Regional Meeting of Sedimentology), 22, p140.

Sun, Q., Chu, G., Liu, G., Li, S., and Wang, X. (2007). Calibration of Alkenone Unsaturation Index with Growth Temperature for a Lacustrine Species, Chrysotila Lamellosa (Haptophyceae). *Org. Geochem.* 38 (8), 1226–1234. doi:10.1016/j.orggeochem.2007.04.007

Sun, W., Zhang, E., Jones, R. T., Liu, E., and Shen, J. (2015). Asian Summer Monsoon Variability during the Late Glacial and Holocene Inferred from the Stable Carbon Isotope Record of Black Carbon in the Sediments of Muge Co, Southeastern Tibetan Plateau, China. *The Holocene* 25 (12), 1857–1868. doi:10.1177/0959683615605743

Sun, W., Zhang, E., Jones, R. T., Liu, E., and Shen, J. (2016). Biogeochemical Processes and Response to Climate Change Recorded in the Isotopes of Lacustrine Organic Matter, Southeastern Qinghai-Tibetan Plateau, China. *Palaeogeogr. Palaeoclimatol. Palaeoecol.* 453, 93–100. doi:10.1016/j.palaeo.2016.04.013

Topal, S., and Özkul, M. (2014). Soft-Sediment Deformation Structures Interpreted as Seismites in the Kolankaya Formation, Denizli Basin (SW Turkey). *Scientific World J.* 2014, 1–13. doi:10.1155/2014/352654

Van Daele, M., Moernaut, J., Doom, L., Boes, E., Fontijn, K., Heirman, K., et al. (2015). A Comparison of the Sedimentary Records of the 1960 and 2010 Great Chilean Earthquakes in 17 Lakes: Implications for Quantitative Lacustrine Palaeoseismology. *Sedimentology* 62 (5), 1466–1496. doi:10.1111/sed.12193

Vandekerkhove, E., Van Daele, M., Praet, N., Cnudde, V., Haeussler, P. J., De Batist, M., et al. (2019). Flood-triggered versus Earthquake-Triggered Turbidites: A Sedimentological Study in Clastic lake Sediments (Eklutna Lake, Alaska). *Sedimentology* 67 (1), 364–389. doi:10.1111/sed.12646

Wang, X., Yu, H., and Pei, X. (1996). Application and Results of Statistic Hazard Data about the 1955 M7.5 Kangding Earthquake. *Earthquake Res. Sichuan* 3, 57–64.

Wang, E., Burchfiel, B. C., Royden, L. H., Chen, L., and Chen, Z. (1998). *Late Cenozoic Xianshuihe-Xiaojiang, Red River, and Dali Fault Systems of Southwestern Sichuan and Central Yunnan, China*, 327. Colorado: The Geological Society of America, Inc. Special Paper, 108.

Wang, S., Jiang, G., Xu, T., Tian, Y., Zheng, D., and Fang, X. (2012). The Jinhe–Qinghe Fault—An Inactive Branch of the Xianshuihe–Xiaojiang Fault Zone, Eastern Tibet. *Tectonophysics* 544, 93–102. doi:10.1016/j.tecto.2012.04.004

Weltje, G. J., Bloemsma, M. R., Tjallingii, R., Heslop, D., Röhl, U., and Croudace, I. W. (2015). "Prediction of Geochemical Composition from XRF Core Scanner Data: A New Multivariate Approach Including Automatic Selection of Calibration Samples and Quantification of Uncertainties,". *Micro-XRF Studies of Sediment Cores*. Editors I. W. Croudace and R. G. Rothwell (Dordrecht: Springer Netherlands), 17, 507–534. doi:10.1007/978-94-017-9849-5_21

Wen, X., Allen, C. R., Luo, Z., Qain, H., Zhou, H., and Huang, W. (1989). Segmentation, Geometric Features, and Their Seismotectonic Implications for the Holocene Xianshuihe Fault Zone. *Acta Seismol. Sin.* 11 (4), 362–372.

Wen, X.-z., Ma, S.-l., Xu, X.-w., and He, Y.-n. (2008). Historical Pattern and Behavior of Earthquake Ruptures along the Eastern Boundary of the Sichuan-Yunnan Faulted-Block, Southwestern China. *Phys. Earth Planet. Interiors* 168 (1-2), 16–36. doi:10.1016/j.pepi.2008.04.013

Wilhelm, B., Arnaud, F., Sabatier, P., Crouzet, C., Brisset, E., Chaumillon, E., et al. (2012). 1400 Years of Extreme Precipitation Patterns over the Mediterranean French Alps and Possible Forcing Mechanisms. *Quat. Res.* 78 (1), 1–12. doi:10.1016/j.yqres.2012.03.003

Wilhelm, B., Nomade, J., Crouzet, C., Litty, C., Sabatier, P., Belle, S., et al. (2016). Quantified Sensitivity of Small lake Sediments to Record Historic Earthquakes: Implications for Paleoseismology. *J. Geophys. Res. Earth Surf.* 121 (1), 2–16. doi:10.1002/2015jf003644

Wilhelm, B., Rapuc, W., Amann, B., Anselmetti, F. S., Arnaud, F., Blanchet, J., et al. (2022). Impact of Warmer Climate Periods on Flood hazard in the European Alps. *Nat. Geosci.* 15 (2), 118–123. doi:10.1038/s41561-021-00878-y

Wils, K., Daryono, M. R., Praet, N., Santoso, A. B., Dianto, A., Schmidt, S., et al. (2021). The Sediments of Lake Singkarak and Lake Maninjau in West Sumatra Reveal Their Earthquake, Volcanic and Rainfall History. *Sediment. Geology.* 416, 105863. doi:10.1016/j.sedgeo.2021.105863

Woodward, C. A., and Gadd, P. S. (2019). The Potential Power and Pitfalls of Using the X-ray Fluorescence Molybdenum Incoherent: Coherent Scattering Ratio as a Proxy for Sediment Organic Content. *Quat. Int.* 514, 30–43. doi:10.1016/j.quaint.2018.11.031

Woodward, C. A., Slee, A., Gadd, P., Zawadzki, A., Hamze, H., Parmar, A., et al. (2018). The Role of Earthquakes and Climate in the Formation of Diamictic Sediments in a New Zealand Mountain Lake. *Quat. Int.* 470, 130–147. doi:10.1016/j.quaint.2017.10.051

Writing Group of Compilation of Sichuan Earthquake Data (1980a). *Compilation of Sichuan Earthquake Data*, Vol. 1. Chengdu: Sichuan People's Publishing House.

Writing Group of Compilation of Sichuan Earthquake Data (1980b). *Compilation of Sichuan Earthquake Data*, Vol. 2. Chengdu: Sichuan People's Publishing House.

Xie, H., Guo, D., Wang, S., and Wei, F. (1997). Flood Causes in Town Proper of Kangding in 1995. *Mt Res.* 1997 (02), 129–131. doi:10.16089/j.cnki.1008-2786.1997.02.014

Xiong, T., Yao, X., and Zhang, Y. (2010). A Review of Activity of Xianshuihe Fault Zone since the Holocene. *J. Geomechan.* 16 (02), 176–188. doi:10.3969/j.issn.1006-6616.2010.02.007

Yan, B., and Lin, A. (2015). Systematic Deflection and Offset of the Yangtze River Drainage System along the Strike-Slip Ganzi-Yushu-Xianshuihe Fault Zone, Tibetan Plateau. *J. Geodynamics* 87, 13–25. doi:10.1016/j.jog.2015.03.002

Yan, B., Wang, M., Jia, D., Cui, J., and Hu, J. (2019). Investigation and Magnitude Re-evaluation of the 1955 Zheduotang Earthquake, Eastern Tibetan Plateau, China. *Geol. J.* 55 (11), 7272–7284. doi:10.1002/gj.3628

Zhang, C., Zhou, A., Zhang, X., Wu, D., and Hao, S. (2015). Identification of Paleaoflood Events by Lacustrine Archives and Their Links to Climatic Conditions. *Prog. Geogr.* 34 (07), 898–908. doi:10.18306/dlkxjz.2015.07.011

Zhou, R., Gong, N., Ma, S., Xia, C., and Li, X. (2001). Evaluation of Possibility of Reservoir-Induced Earthquake at Mugeco Lake Hydropower Station. Des. *Hydroelectr. Power Station* 17 (02), 81–88. doi:10.3969/j.issn.1003-9805.2001.02.026

Conflict of Interest: The authors declare that the research was conducted in the absence of any commercial or financial relationships that could be construed as a potential conflict of interest.

Publisher's Note: All claims expressed in this article are solely those of the authors and do not necessarily represent those of their affiliated organizations, or those of the publisher, the editors, and the reviewers. Any product that may be evaluated in this article, or claim that may be made by its manufacturer, is not guaranteed or endorsed by the publisher.